IEEE Access
Multidisciplinary | Rapid Review | Open Access Journal

Received June 18, 2017, accepted August 7, 2017, date of publication August 23, 2017, date of current version September 19, 2017.

Digital Object Identifier 10.1109/ACCESS.2017.2740967

Magnetic Nanoparticle-Guided Blind Focusing of the Electric Field for Microwave Hyperthermia

GENNARO BELLIZZI AND OVIDIO MARIO BUCCI, (Life Fellow, IEEE)
DIETI, University of Naples Federico II, 80125 Naples, Italy
IREA-CNR, 80124 Naples, Italy
CNIT, 43124 Parma, Italy

Corresponding author: Gennaro Bellizzi (gbellizz@unina.it)

ABSTRACT This paper deals with microwave hyperthermia, presenting a novel way to achieve the blind focusing on the tumor of the electric field radiated by an array of antennas. As in a recently proposed approach, the idea is to determine the antenna excitations by measuring the variation of the electric field arising from a localized variation of the electromagnetic contrast, without requiring any *a priori* knowledge of the geometry and of the electric properties of the tissues wherein the electromagnetic field propagates (thus, the adjective ''blind''). The first novelty of the new approach is the use of magnetic nanoparticles as contrast agents, which, in addition to being biocompatible, are appealing thanks to the possibility of changing their magnetic contrast, in a fast, remote, and reversible way, by applying an external magnetic field. This allows a reconfigurable focusing through a continuous tuning of the antenna excitations, thereby enabling one to counteract the possible loss of focusing that could occur during the treatment. However, the magnetic nature of the induced contrast variation requires the development of *ad hoc* strategies for the synthesis of the excitations, which represent the other novelty of the new approach. Its effectiveness has been thoroughly investigated with an exhaustive 2-D numerical analysis, considering as case study that of breast cancer, and further assessed through 3-D realistic numerical simulations.

INDEX TERMS Microwave hyperthermia, blind focusing, contrast agents, magnetic nanoparticles.

I. INTRODUCTION

Microwave Hyperthermia (MH) is a modality of cancer thermotherapy, where the selective heating of the tumor tissue is achieved by focusing the electric field (EF) radiated by an array of antennas external to the region of interest (ROI), operating at microwave frequencies [1], [2].

Once the array layout (i.e. number, location and type of radiating elements) has been set, the problem in MH is to determine the excitations of the antennas ensuring the focusing of the EF on the tumor, while avoiding hot spots in the surrounding healthy tissue. To this end, several synthesis strategies can be adopted, the simplest (and probably the first) being those based on the time reversal (TR) principle [3], [4].

Since then, more sophisticated and performing methods have been proposed, all based on an unconstrained or constrained optimization of a proper objective functional of the antenna excitations [5]–[10].

However, all these approaches require a more or less accurate knowledge of the geometry and of the electric properties of the ROI, not always available. For instance, the geometry and the internal structure of the ROI are usually acquired at the diagnostic stage, through a MRI or a CT scan. And so, they can be significantly different from those occurring at the therapeutic stage, because the positions of the patient during the MRI or CT and during the hyperthermia session are not the same. This is particularly true for those parts of the human body, like the breast, which are easily deformable.

Even higher can be the uncertainty on the values of electric properties assigned to the different types of tissue. Indeed, they are derived from measurements on *ex vivo* tissue samples. Therefore, they are neither patient specific nor take into account the influence of *in vivo* functions, like the bloodstream. In addition, one must take into account that both the geometry and the electric properties of the ROI can change during the treatment (the former, due to possible movements of the patient, the latter due to the variation of the electric properties with the temperature increase), thus leading to a progressive loss of focusing.

In the light of above considerations, approaches that are *blind* (namely do not require any a priori knowledge on

the ROI properties) and possibly *reconfigurable* are of interest.

Inspired by the new frontier of *theranostics*, a blind approach has been recently proposed [11], where the information required for the field focusing is directly measured by the same antenna array employed in the treatment, at a ''diagnostic'' stage previous to the treatment.

This approach exploits nano-composites, like micro-bubbles or carbon nano-tubes, as contrast agents, locally supplied to the tumor, in order to induce a detectable variation of the electric contrast of the tumor. The antenna excitations are then determined by measuring (and processing) the variation of the EF arising from the variation of the electric contrast of the tumor, without requiring any *a priori* knowledge on the geometry and on the electric properties of the ROI, as well as on its position with respect to the antenna array. The main drawback of this approach is that, once infused, the electric properties of such nano-composites cannot be modified, therefore, the electric contrast of the tumor can be changed only once: when the nano-composites are inserted into it. Moreover, the approach is sensitive to any other variation of the electric scenario which could occur between the measurements of the EF performed before and after the injection of the contrast agent (e.g., due to the breathing, the heartbeat and so on).

As in the case of microwave imaging [12], a possible way to overcome these drawbacks has been very recently proposed, namely the use of magnetic nano-particles (MNP) as contrast agents [13].

First of all, MNP are appealing because they can be made biocompatible and are currently adopted as contrast agents in MRI. Concerning the therapeutic application, in the European Union their use is approved in the hyperthermic treatment of brain and prostate cancer, and is under consideration in the United States of America [14]. Secondly, MNP can be directly supplied to the tumor (in form of colloidal suspension) through a direct injection, which has the advantage to be both minimally invasive and to allow the accumulation of a large amount of MNP (hundreds of mg of MNP), thus enabling to induce a remarkable (i.e. well detectable) magnetic contrast variation of the tumor [15], [16]. Moreover, once injected, MNP spread out very slowly in the surrounding tissues, so that they remain concentrated into the tumor for long time, thus allowing the application of multiple sessions of hyperthermia without the need of re-injecting them. Last, but not least, their microwave magnetic contrast can be changed, in a fast (much faster than the rate characterizing the breathing, the heartbeat or any other movement), remote and reversible manner, by applying an external polarizing magnetic field (PMF) [15], [16]. This feature makes the blind focusing scarcely sensitive to the variations of the scattered field not due to the injected contrast agent. Moreover, it allows an online and continuous tuning of the antenna excitations (hence a reconfigurable focusing of the EF), thus enabling one to counteract possible loss of focusing due to changes of the electric scenario of the ROI during the treatment, in particular those due to the temperature variations.

However, due to the magnetic nature of the contrast variation induced by the MNP, one cannot exploit the procedure devised in [11] for the synthesis of the antenna excitations, as it works for a localized *electric* contrast change and not for a *magnetic* contrast variation. Indeed, as shown in [11], in this case the field focused on the tumor would be the magnetic field (MF) rather than the EF, as required.

Hence, the first aim of this paper is to provide a sound mathematical framework to the problem of determining the excitations required for blindly focusing the EF by exploiting the measured *differential scattering matrix* (DSM), resulting from the variation of the MNP magnetic contrast induced by an applied PMF. This allows not only to elucidate the synthesis strategy already suggested in [13], assessing the assumptions lying at its basis, but also to develop a novel strategy, analogue to that presented in [11], which estimates the antenna excitations as a specific higher order singular vector of the singular value decomposition (SVD) [17] of the DSM. The effectiveness of both the synthesis strategies has been numerically tested in the case of a 2D geometry, exploiting as model a slice of a realistic human breast. A comprehensive comparison between the two strategies and a standard TR approach is also provided. Moreover, their robustness against the measurement noise has been assessed. Finally, we report the results of a 3D analysis, carried out by using the same breast model, which confirm the effectiveness of the proposed approach.

The paper is organized as follows. The formulation of the problem and the theoretical background underlying our approach are reported in Section II. The devised synthesis strategies are presented in Section III. The results of the numerical analysis aimed at assessing the performance of the proposed approach are reported in Section IV. Conclusions follow in Section V.

II. FORMULATION OF THE PROBLEM AND THEORETICAL BACKGROUND

The conceptual scheme of the MNP-guided FMH is shown in Fig. 1. As already said, the approach relies on the measurement of the DSM, say $\underline{\underline{S}}$, resulting from the variation of the magnetic contrast of the MNP in the tumor induced by switching ''on'' and ''off'' an applied PMF [12].

From the electromagnetic point of view, the system is made of an array of N (Tx/Rx) antennas located on an ''observation'' surface (Σ in Fig. 1), radiating in presence of an electrically inhomogeneous medium. This last consists of the tumor tissue containing the MNP, say Ω_t, plus the surrounding healthy tissue, say Ω, and the background medium (BM), wherein the ROI and the antennas are embedded. Later on, an $\exp(i\omega t)$ time dependence will be assumed and dropped, ω being the angular frequency and i the imaginary unit.[1]

[1] All the results can be extended to the multi-frequency case

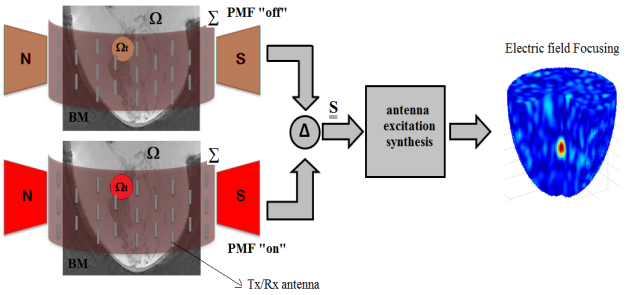

FIGURE 1. Conceptual scheme of MNP-guided focused microwave hyperthermia.

Now, let us denote with $\varepsilon(\mathbf{r})$ the equivalent permittivity of the medium and with $\chi(\mathbf{r})$ the *variation* of the magnetic contrast (namely, the relative magnetic susceptibility) of the MNP in the tumor due to the switching of the applied PMF, $\mathbf{r}$ being the position vector with respect to a fixed Cartesian reference frame. For convenience, without any loss of generality, the origin of the frame is assumed in the barycenter of the MNP distribution. The *difference*, say $(\mathbf{E}_n, \mathbf{H}_n)$, of the fields scattered by the MNP, before and after the variation of their magnetic contrast, when the impinging field on the MNP is that generated by the n-th Tx antenna, is solution of the Maxwell's equations [11]:

$$\nabla \times \mathbf{E}_n(\mathbf{r}) = -i\omega\mu_0 \mathbf{H}_n(\mathbf{r}) - \mathbf{M}_n(\mathbf{r}) \tag{1}$$

$$\nabla \times \mathbf{H}_n(\mathbf{r}) = i\omega\varepsilon(\mathbf{r})\,\mathbf{E}_n(\mathbf{r}) \tag{2}$$

In (1)-(2) μ_0 is the free space permeability and $\mathbf{M}_n$ is the *variation* of the equivalent magnetic current induced in Ω_t by the presence of the MNP. In the case of electrically small tumors and weak magnetic contrast variations, like those achievable with a tolerable amount of MNP, the following expression can be confidently assumed for $\mathbf{M}_n$ (distorted Born approximation):

$$\mathbf{M}_n(\mathbf{r}) = i\omega\mu_0\chi(\mathbf{r})\,\mathbf{H}_n^i(\mathbf{r}) \tag{3}$$

where $\mathbf{H}_n^i$ is the MF generated by the n-th Tx antenna and impinging in Ω_t (i.e. the field in *absence* of the magnetic anomaly). As a result, the difference, say V_m^-, of the signals received by the m-th Rx antenna, due to $\mathbf{M}_n$ induced in Ω_t, apart from an unessential constant factor, is given by:

$$V_m^- = V_n^+ \int_{\Omega t} \mathbf{H}_m^i(\mathbf{r}) \cdot \mathbf{M}_n(\mathbf{r})\, d\mathbf{r} \tag{4}$$

where V_n^+ is the amplitudes of the incident wave feeding the n-th Tx antenna and $\mathbf{H}_m^i$ is the pertinent magnetic Green function of the medium (including the presence of the antennas and, possibly, their coupling), which, by reciprocity, coincides with the MF radiated in Ω_t by the m-th antenna when operating in Tx mode. Accordingly, by replacing (3) in (4) and dividing by V_n^+, we obtain the following expression for the generic entry of $\underline{\underline{S}}$:

$$s_{m,n} = \int_{\Omega t} \chi(\mathbf{r})\,\mathbf{H}_m^i(\mathbf{r}) \cdot \mathbf{H}_n^i(\mathbf{r})\, d\mathbf{r} \tag{5}$$

Now, by virtue of the assumption of electrically small tumor, we can expand the dot product between the MF in (5) in Maclaurin's series and truncate the expansion to the second order term in $\mathbf{r}$. By doing so, and assuming a spherically symmetric distribution for $\chi(\mathbf{r})$ in Ω_t (this is a quite reasonable assumption in that, once injected, the MNP tend to spread uniformly in all directions, in the surrounding tissue [18]), we obtain the following expression for $s_{m,n}$ (see Appendix):

$$\begin{aligned} s_{m,n} \cong \int_{\Omega t} \chi(\mathbf{r})\, d\mathbf{r} \Big(& (1 - \frac{1}{5}(k_t R)^2)\mathbf{H}_m^i(\mathbf{0}) \cdot \mathbf{H}_n^i(\mathbf{0}) \\ & - \frac{(k_t R)^2}{10\zeta_t^2}\mathbf{E}_m^i(\mathbf{0}) \cdot \mathbf{E}_n^i(\mathbf{0}) + \frac{(k_t R)^2}{20\, k_t^2} \sum_{q=1}^{3} \mathbf{i_q} \\ & \cdot \nabla_s \mathbf{H}_m^i(\mathbf{0}) \cdot \nabla_s \mathbf{H}_n^i(\mathbf{0}) \cdot \mathbf{i_q} \Big) \end{aligned} \tag{6}$$

In (6), R denotes an "effective" radius of the MNP distribution, whose maximum value (attained in the case of uniform distribution) is equal to the radius of Ω_t, k_t and ζ_t are the propagation constant and the characteristic impedance of the medium at $\mathbf{r}=\mathbf{0}$, $\mathbf{i_q}$ is the unit vector along the x_q-axis of the reference frame (q=1, 2, 3). Moreover, $(\mathbf{E}_{n[m]}^i, \mathbf{H}_{n[m]}^i)$ is the incident field radiated by the n[m]-th antenna and $\nabla_s \mathbf{H}_{n[m]}^i$ is the symmetric part of the Jacobian matrix, $\nabla \mathbf{H}_{n[m]}^i$, of the incident MF radiated by the n[m]-th antenna. Notice that, because $\chi(\mathbf{r})$ is proportional to the MNP concentration, the value of the integral in (6) only depends on the total amount of MNP in Ω_t.

From (6), one can immediately see that, up to the retained order in $k_t R$, $\underline{\underline{S}}$ is the sum of three symmetric matrices. The dominant matrix, say $\underline{\underline{S}}_{H0}$, is related to the magnetic dipole moment (first term in (6)) of the equivalent magnetic current variation induced in Ω_t by the variation of the PMF. The two second order matrixes, say $\underline{\underline{S}}_{E2}$ and $\underline{\underline{S}}_{H2}$, are related to the electric dipole (second term in (6)) and the magnetic quadrupole (third term in (6)) moments, respectively, of such current variation. $\underline{\underline{S}}_{H0}$ is at most a matrix of rank three,[2] so that it has at most three singular values different from zero, to which three singular vectors do correspond. The MF radiated by the antenna array when fed by each of such singular vectors are the three different ways (along three orthogonal directions of the space) whereby the MF can be focused in Ω_t. The same holds for $\underline{\underline{S}}_{E2}$, but with reference to the EF. Instead, $\underline{\underline{S}}_{H2}$ is at most a matrix of rank six (equal to the number of independent elements of $\nabla_s \mathbf{H}_{n[m]}^i(\mathbf{0})$), so that it has at most six singular values different from zero.

The following considerations are now in order. The singular vectors corresponding to the non-null singular values of $\underline{\underline{S}}_{H0}$ are expected to be (nearly) orthogonal to those of $\underline{\underline{S}}_{E2}$ and $\underline{\underline{S}}_{H2}$. The same is expected for the singular vectors of $\underline{\underline{S}}_{E2}$ and $\underline{\underline{S}}_{H2}$. The first statement can be inferred by noting that when the MF is focused in Ω_t, its spatial derivatives in Ω_t are negligible and so are negligible the electric dipole and the

[2] $\underline{\underline{S}}_{H0}$ is the sum of three matrixes of rank 1, each corresponding to one of the three term of the dot product of the MF defining $\underline{\underline{S}}_{H0}$.

magnetic quadrupole terms, which are related to the Jacobian matrix of the MF impinging in Ω_t. The second result can be inferred by noting that when the EF is focused in Ω_t, for symmetry, the MF lines wind around the focusing point and lie in the plane orthogonal to the EF direction. For such a MF it is easy to show that the symmetric part of the Jacobian matrix at the focusing point, hence the quadrupole moment, is (nearly) zero.

Accordingly, we can foresee that the first non-null singular values of $\underline{\underline{S}}$ are practically coincident with those of $\underline{\underline{S}}_{H0}$, $\underline{\underline{S}}_{E2}$ and $\underline{\underline{S}}_{H2}$. Moreover, the smaller is $|k_t R|$, the smaller are the singular values of $\underline{\underline{S}}_{E2}$ and $\underline{\underline{S}}_{H2}$ as compared to those of $\underline{\underline{S}}_{H0}$, being $\underline{\underline{S}}_{E2}$ and $\underline{\underline{S}}_{H2}$ of second order in $k_t R$ as compared to $\underline{\underline{S}}_{H0}$. Therefore, for electrically small tumors, the curve of the singular values of $\underline{\underline{S}}$ is expected being characterized by an abrupt drop (knee) delimiting the transition between the singular values of $\underline{\underline{S}}_{H0}$ and those of $\underline{\underline{S}}_{E2}$ and $\underline{\underline{S}}_{H2}$.

Above considerations lie at the basis of the synthesis strategies to determine, from the measurement of $\underline{\underline{S}}$, the vector of the antenna excitations, allowing to focus the EF on the tumor, without requiring any *a priori* knowledge of the geometry and of the electric properties of the ROI, as well as of its position with respect to the antenna array.

III. SYNTHESIS STRATEGIES

As already stressed in the Introduction, because $\underline{\underline{S}}$ is dominated by the magnetic dipolar contribution, -see (6)-, we cannot set as excitation vector the dominant singular vector of $\underline{\underline{S}}$, as done in [11], because this would determine the focusing of the MF rather than the EF [11]. Therefore, in order to deal with MNP an *ad hoc* synthesis strategy must be devised. In the next sub-sections we will present two different strategies.

The first one, say strategy A, is that proposed in [13] and is here revisited and described in detail. It determines the excitation vector, say $\boldsymbol{e}$, by processing the elements of the main diagonal of $\underline{\underline{S}}$.

The second new, strategy, say strategy B, determines $\boldsymbol{e}$ as the singular vector of $\underline{\underline{S}}$ corresponding to the electric dipole moment of the equivalent magnetic current variation in Ω_t.

A. STRATEGY A

As anticipated, this strategy determines $\boldsymbol{e}$ from the elements of the main diagonal[3] of $\underline{\underline{S}}$. According to (6), at the zero order in $k_t R$, they are given by:

$$s_{n,n} \cong \int_{\Omega_t} \chi(\mathbf{r})\, d\mathbf{r} \mathbf{H}_n^i(\mathbf{0}) \cdot \mathbf{H}_n^i(\mathbf{0}) \tag{7}$$

Let us notice that, independently of the magnitude of $\mathbf{H}_n^i(\mathbf{0})$ and/or the magnitude of $\chi(\mathbf{r})$, $s_{n,n}$ is zero if $\mathbf{H}_n^i(\mathbf{0})$ is circularly polarized, being zero the dot product of $\mathbf{H}_n^i(\mathbf{0})$ by itself. Therefore, a mandatory requirement for the application of strategy A is that the eccentricity of the polarization ellipse of $\mathbf{H}_n^i(\mathbf{0})$ is sufficiently different from zero, and it is expected that it works better the nearer to 1 is the eccentricity (i.e. $\mathbf{H}_n^i(\mathbf{0})$ almost linearly polarized). The fulfillment of such condition requires, at least, the employment of linearly polarized antennas. Under above polarization condition, $s_{n,n}$ is then (almost) proportional to the square of the complex phasor of $\mathbf{H}_n^i(\mathbf{0})$.

If we further assume that the field behaves locally as a plane wave, $s_{n,n}$ will be also proportional to the square of the complex phasor of the corresponding EF, $\mathbf{E}_n^i(\mathbf{0})$, which is the sought quantity. Accordingly, under the above hypotheses, by applying the TR principle [3], the n-th component of the (normalized) excitation vector $\boldsymbol{e}$ (i.e., the excitation of the n-th antenna of the array) is given by:

$$e_n = \pm \sqrt{(s_{n,n})^*} / \|\boldsymbol{e}\|_2 \tag{8}$$

where the complex conjugation "$*$" corresponds in the frequency domain to a TR in the time domain (as usual, in (8) the symbol $||\cdot||_2$ denotes the L_2 norm).

As the sign of e_1 can be arbitrarily set, there are 2^{N-1} possible ways of choosing the signs in (8). Of course, only one of them provides the right excitation vector, say $\boldsymbol{e}_A$, required to focus the EF onto Ω_t. To find $\boldsymbol{e}_A$, let us notice that, if we do not want to limit *a priori* the focusing capability of the array, the angular distance between its elements cannot be much larger than that between the sampling points required to suitably represent over Σ the field radiated by an arbitrary source in Ω [19]. This last is of the order of $\lambda_b/2R_\Omega$, where λ_b is the wavelength in BM and R_Ω the radius of the smallest sphere enclosing Ω [20]. Because in all practical instances the size of Ω is larger than λ_b, it is expected that if the MF radiated by two adjacent antennas interfere constructively in Ω_t, the same do the EF, which is just the condition we have to meet to focus the total EF in Ω_t. This allows to determine $e_{A,n}$ ($n = 2, \ldots, N$), from the previously estimated $e_{A,n-1}$, by choosing the sign of $e_{A,n}$ in such a way that the MF radiated by the n-th and the (n-1)-th antennas interfere constructively in Ω_t.

Now, the *differential* scattered field measured on Σ is proportional to the MF impinging on Ω_t, see (3). Accordingly the condition of constructive interference can be meet by evaluating the norm of the *differential* field scattered by the MNP for the two excitation vectors $\boldsymbol{e}_n^{\pm} = (0, \ldots, 0, e_{A,n-1}, \pm e_n, 0, \ldots, 0)$, which differ from each other for the sign of e_n, and looking for the maximum. This leads to the following recursive schema for the choice of $e_{A,n}$:

$$e_{A,n} = argmax\left(\left\|\underline{\underline{S}}\boldsymbol{e}_n^-\right\|_2, \left\|\underline{\underline{S}}\boldsymbol{e}_n^+\right\|_2\right) \tag{9}$$

which allows to determine $\boldsymbol{e}_A$ starting from $e_{A,1}$, whose sign, as previously noted, can be arbitrarily chosen.

Should the adopted array have a number of elements significantly lower than that required to ensure a full

[3]The main diagonal of $\underline{\underline{S}}$ can be directly measured or estimated by performing the SVD of $\underline{\underline{S}}$ and then by summing the Hadamard products of the singular vectors by themselves, times the corresponding singular values. Possibly, the sum could be limited to the dominant singular values.

re-configurability, possibly impairing the reliability of the above recursive procedure, a different (and computationally more demanding) approach could be exploited to set $\boldsymbol{e}_A$. To this end, let us note that if the EF radiated by the array is focused in Ω_t, the norm of the corresponding MF in Ω_t is expected being minimum. As a result, also the norm of the magnetic current variation induced in Ω_t, hence, the norm of the corresponding differential field scattered by the MNP and measured by the antenna array will be minimum. Accordingly, we have:

$$\boldsymbol{e}_A = argmin\left(\left\|\underline{\underline{S}}\boldsymbol{e}\right\|_2\right) \tag{10}$$

Due to its intrinsic discrete nature, some kind of genetic optimization algorithm could be profitably adopted to face the optimization problem defined in (10).

B. STRATEGY B

As all the information required for focusing the EF on the tumor is contained in the electric dipolar term $\underline{\underline{S}}_{E2}$, this strategy determines the antenna excitations by extracting such contribution from $\underline{\underline{S}}$. This goal can be successfully achieved by exploiting the results on the SVD of $\underline{\underline{S}}$ inferred in Section II.

According to these results, for an electrically small tumor ($|k_t R| \ll 1$), the first non-null singular values (and the corresponding singular vectors) of $\underline{\underline{S}}$ are essentially coincident with those of the terms $\underline{\underline{S}}_{H0}$, $\underline{\underline{S}}_{E2}$ and $\underline{\underline{S}}_{H2}$. Moreover, due to different order in $k_t R$ of such terms, the curve of the singular values of $\underline{\underline{S}}$ is expected to exhibit a knee, where the singular values before the knee (the highest ones) are related to $\underline{\underline{S}}_{H0}$, while the singular values immediately after are essentially those of $\underline{\underline{S}}_{E2}$ and $\underline{\underline{S}}_{H2}$. The excitation vector, say $\underline{\boldsymbol{e}}_B$, is then one of the singular vectors associated to the singular values immediately after the knee. Since it is reasonably expected that the electric dipolar term is dominant as compared to the magnetic quadrupolar term, the sought $\underline{\boldsymbol{e}}_B$, is that associated to the first singular value after the knee.

As a concluding remark, we would like to stress that, like in [11], strategy B relies on the individuation of the dominant singular value of the electric dipolar term $\underline{\underline{S}}_{E2}$ of $\underline{\underline{S}}$. The substantial difference with the approach in [11] is that in the case of a localized variation of the electric contrast of the tumor, as in [11], this task is straightforward, being $\underline{\underline{S}}$ practically coincident with the sought electric dipolar term. Conversely, in the case at hand, the electric dipolar contribution is of higher order with respect to the magnetic dipolar one, so that its retrieving is not as trivial as in [11] and has, therefore, required an accurate analysis and physical interpretation of the SVD of $\underline{\underline{S}}$ for its correct individuation.

C. COMPARISON BETWEEN STRATEGIES A AND B

As strategies A and B perform a different processing of $\underline{\underline{S}}$ and rely on different requirements, it is expected that their performance can be different, depending on the case at hand.

Strategy A, while relying on assumptions whose fulfillment is difficult to assess *a priori*, exploits the dominant term of $\underline{\underline{S}}$, hence requires a signal-to-noise ratio (SNR) lower than strategy B, which, instead, exploits a higher order term of $\underline{\underline{S}}$. This is especially true for tumors of small size. Therefore, it could happen that the available SNR is suitable for an estimation of the excitations through strategy A, but not through strategy B.

On the other hand, strategy B, relying on less restrictive assumptions than strategy A, is expected to provide reliable results in a wider range of cases than strategy A.

Confidently, this should not be the case in hyperthermia where the MNP can be directly injected into the tumor, thus enabling the accumulation of an amount of hundreds mg of MNP [21], [22] much larger than the one that has been successfully detected by using standard (i.e., cheap) MWI systems, of some mg of MNP [23], [24].

This makes the implementation of both strategies a concrete possibility. In this respect, it is worth noting that, as the two strategies rely on different assumptions, the agreement of their results is a good indicator of reliability. Moreover, they could be properly combined together in order to increase their effectiveness. For instance, one can use strategy A to obtained a preliminary estimation of the excitation vector to be used for a more precise individuation of the singular vector of $\underline{\underline{S}}$ associated to the electric dipole moment of the induced magnetic current variation.

IV. NUMERICAL ANALYSIS

To test the effectiveness of the proposed synthesis strategies, we have carried out a numerical analysis, by considering as case study that of breast cancer. In order to assess their performance with respect to the tumor position and the robustness against measurement noise (even if this latter is expected to be not a critical point for the reasons outlined in Section III-C), a simplified 2D numerical analysis has been firstly carried out, whose results complement and confirm those reported in [13]. A comparison between the two strategies and a standard TR approach is also provided.

Then a 3D analysis has been carried out, whose results allows assessing the effectiveness of both the synthesis strategies in a realistic operative scenario.

A. 2D SIMULATION SET-UP

As breast model, we have exploited the realistic numerical phantoms of the online repository available at [25]. To test the focusing performance of the strategies in the worst case, an anatomically (and electromagnetically) dense breast (phantom ID 062204) has been considered. The 2D scenario has been obtained by extracting a slice from the 3D original phantom at a frequency of 1 GHz, the working frequency. Since this phantom is relative to a healthy patient, a circular tumor of 1 cm in size has been inserted, at the position positions $(0, -2)$ cm. They are shown in Fig. 2. The values

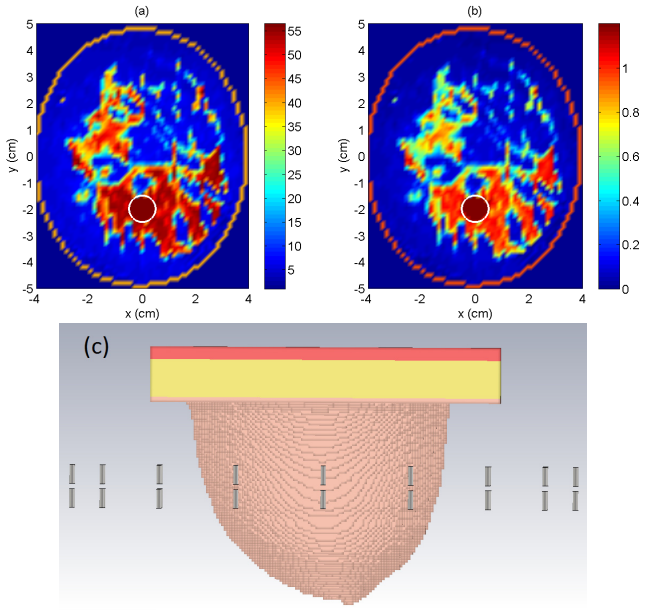

FIGURE 2. Relative permittivity (a) and effective electric conductivity (b) maps, at 1 GHz, of the 2D breast phantom (white circles bound the tumor) (c) A view of the 3D breast model in CST environment.

assumed for the electric properties of the tumor are about 15% larger than those found for normal fibro/glandular tissue [26]. The assumed magnetic contrast variation in the tumor is $\chi = 0.015 - i0.025$. This value was found experimentally for a sample of magnetite nanoparticles, of 10 nm in size, dispersed in water at a concentration of 17.5 mg Fe/mL [16]. Notice that the choice of the working frequency is a trade-off between the need of maximizing the MNP contrast (hence the SNR) and the need of satisfying the conditions underlying strategies A and B.

As BM, we have considered distilled water (relative permittivity $\varepsilon_b = 78$ and effective conductibility $\sigma_b = 0.23$ S/m at 1 GHz), as this is the liquid usually employed as refrigerant in hyperthermia, in order to preserve both the skin and healthy tissue from excessive overheating.

The antenna array is made of ideal z-directed currents wires,[4] equally spaced along a ring of radius $R_\Sigma = 10$ cm, surrounding the breast. The number, N, of antennas has been set according to the theory of the degrees of freedom of the electromagnetic field [20], which prescribes $N \approx 2|k_b R_\Omega|$ for an accurate and not redundant representation of the field on the observation line. Assuming $R_\Omega = 4.5$ cm, at 1 GHz, $N = 18$.

B. 3D SIMULATION SET-UP

The 3D simulations have been performed with the aid of the CST Microwave Studio (trial version, kindly provided by the Computer Simulation Technology AG, Darmstadt, Germany). The breast model, the BM, the working frequency, the number of antennas and the MNP concentration are the same as is the 2D analysis. For brevity, only one (spherical) tumor of 1 cm in size, located at (1, −1, 0) cm, has been considered, to which correspond a total amount of injected MNP of about $m_0 = 9$ mg Fe. This amount is well below the dosages employed in the clinical trials for the treatment of brain tumors (112÷616 mg Fe [21]) and prostate tumors (56÷1300 mg Fe [22]).

The whole system is enclosed in a bounding box of size 10 $\lambda_b \times 10\lambda_b \times 6\lambda_b$, λ_b being the wavelength in the BM. Each face of the box is located at a minimum distance of 2 λ_b from the antennas and the breast. Moreover, on each face we have set an absorbing (i.e. open) boundary condition.

C. 2D RESULTS

Fig. 3 shows the (normalized) electric power distribution $p_e(\mathbf{r})$[5] dissipated in the breast, which represents the quantity of actual interest in hyperthermia. In particular, panels (a) and (b) are relative to strategy A and strategy B, respectively. For comparison, in panel (c), we report the results obtained by applying the TR approach, namely by estimating the antenna excitations as the complex conjugate of the EF radiated by a proper elementary electric dipole located at the tumor center and evaluated at the antenna positions. By virtue of the reciprocity, these excitation are determined by computing, for each Tx antenna, the EF radiated at the tumor center (this obviously requires the knowledge of the electric scenario representing the ROI), building the matrix of the EF, $\underline{S}_{E2}$ in (6), and, finally, determining the first singular vector of such matrix (which is equivalent to consider the complex conjugate of the EF samples evaluated at the antenna positions).

As it can be seen, an energy dissipation highly localized in the tumor is obtained with both the strategies. Moreover, these results compare very well with those obtained by the TR approach. From Fig. 3, one can also notice that some "hot spots" take place, but they are unavoidable, at least by adopting an unconstrained synthesis, as they are also present in the TR results.

Even better results, not reported for brevity, have been observed in the case of anatomically (and electromagnetically) less dense breast models.

Fig. 4 shows normalized amplitudes (panel a) and phases (panel b) of the estimated excitation vectors $\boldsymbol{e}_\mathbf{A}$ (red lines) and $\boldsymbol{e}_\mathbf{B}$ (black lines). Again for comparison, we also report the normalized amplitudes and phases of the excitation vectors, say $\boldsymbol{e}_\mathbf{TR}$, estimated by applying the TR approach (blue lines). As it can be seen, both $\boldsymbol{e}_\mathbf{A}$ and $\boldsymbol{e}_\mathbf{B}$ compare very well to $\boldsymbol{e}_\mathbf{TR}$, especially the phases (which are the quantities mainly affecting the focusing of the EF), thus further indicating the effectiveness of the proposed synthesis strategies.

Fig. 4(c) shows, for two different tumor sizes, 10 and 16 mm, the singular values of $\underline{S}$, normalized to the first

[4]Each antenna radiates a TM wave, i.e. a wave having a single component of EF (along the z-axis), and two component of MF (lying in the x-y plane). Therefore, the original 3D vector problem reduces to a simpler 2D scalar problem, having the total EF always only one component along the z-axis.

[5]$p_e(r) = \sigma(r)|E(r)|^2/2$, $\sigma(\mathbf{r})$ being the effective conductivity of the breast model and $|E(r)|$ the magnitude of the EF radiated in the breast

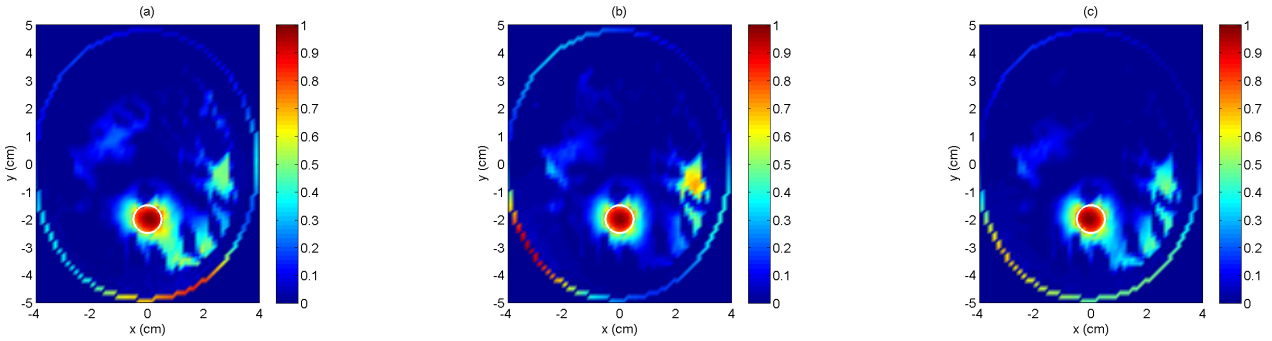

FIGURE 3. Normalized electric power distribution dissipated in the breast: (a) strategy A; (b) strategy B; (c) TR. White circles delimit the tumor.

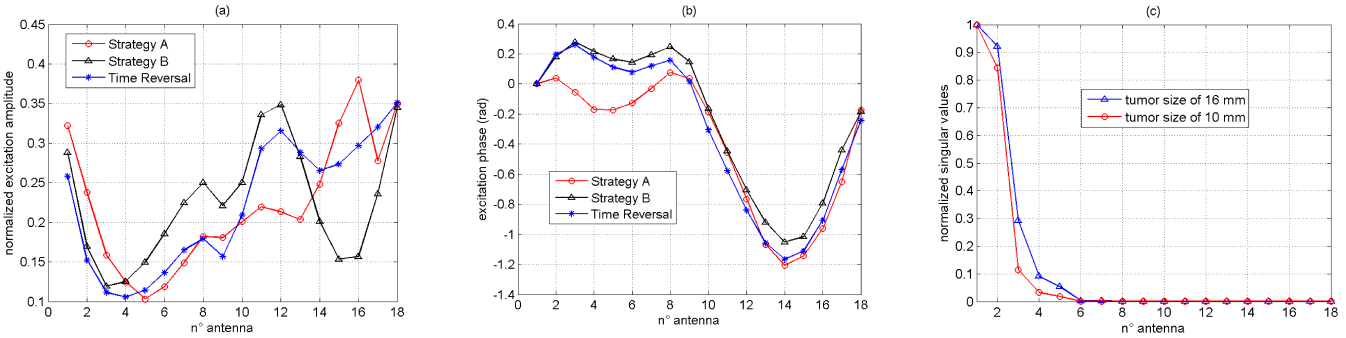

FIGURE 4. Normalized amplitudes (a) and phases (b) of the antenna excitations. Panel (c) shows the normalized singular values of the differential scattering matrix: for two different tumor sizes.

(i.e. the largest) one. As expected - see Section II - there are two dominant singular values, related to the magnetic dipolar term in (6). Instead, the third singular value is significantly smaller as compared to the first two and is related to the electric dipolar term of (6).[6] Moreover, the smaller is tumor the smaller is the third singular value, in agreement with the result in (6) that the third singular value is of second order in $k_t R$.

A synthetic, and quite natural, measure of the focusing performance in FMH is given by the parameter:

$$D = \frac{\frac{1}{\Omega_t}\int_{\Omega_t} p_e(\mathbf{r})d\mathbf{r}}{\frac{1}{\Omega}\int_{\Omega} p_e(\mathbf{r})d\mathbf{r}} \tag{11}$$

namely the ratio between the mean electric power densities dissipated in the tumor and in the whole exposed healthy tissue, respectively (D can be seen as an extension of the well-known concept of directivity of an antenna to the case at hand). Moreover, since in MH one is also interested to keep low the secondary peaks of p_e, in order to avoid harmful hot spots in the healthy tissue, another significant parameter to take into account is the "side lobe level":

$$SL = \min_{\Omega_f \subseteq \Omega/\Omega_t} \left\{ \frac{\frac{1}{\Omega_t}\int_{\Omega_t} p_e(\mathbf{r})d\mathbf{r}}{\frac{1}{\Omega_f}\int_{\Omega_f} p_e(\mathbf{r})d\mathbf{r}} \right\} \tag{12}$$

[6]Of course, in the considered 2D TM case, there are two magnetic dipolar terms and only one electric dipolar term.

where Ω_f is a domain of Ω having the same shape and volume as Ω_t, but not intersecting Ω_t. In other words, SL compares the mean electric power dissipated in the tumor with that dissipated in any other region of the ROI having same shape and size of the tumor. Of course, the larger are D and SL the better is the focusing performance.

Table I reports D and SL for 10 different tumor positions in the breast, including the one in Fig. 2. From the results in Table I one can notice that in all the considered cases a value of D larger than 10 is obtained, indicating that the mean electric power density dissipated in the tumor is at least one order of magnitude larger than that dissipated in the exposed healthy tissue. Accordingly, it is confirmed that both the strategies allow a highly localized energy dissipation in the tumor. Moreover, for both the strategies, the values of D compare very well with those of the TR approach, which is the best one can do, in a completely unconstrained approach.

Regarding SL, except for cases 1 and 10, values not smaller than 2.5 are obtained for all the considered tumor positions. This means that the mean $p_e(\mathbf{r})$ dissipated in the tumor is at least 2.5 times that dissipated in any other region of Ω having same volume and shape as the tumor. To check if this is enough to avoid the occurrence of harmful hot spot would require the solution of the bio-heat equation for the thermal transport, which is outside the purpose of this paper. However, by assuming, as a rough estimate, that the temperature raise in proportional to the heat power delivered to Ω_f (this is quite

TABLE 1. Estimated *D* and *SL* for different tumor positions in the breast (tumor size of 1 cm).

case	Tumor position (cm)	*D* strategy A	*D* strategy B	*D* TR approach	*SL* strategy A	*SL* strategy B	*SL* TR approach
1	(0, -2)	10.0	10.1	11.6	1.9	1.7	2.5
2	(0, 0)	11.6	12.4	13.2	3.3	3.0	2.3
3	(1, 1)	16.9	18.0	19.9	5.0	4.7	6.3
4	(-1, 0)	10.3	13.3	14.2	2.8	3.9	2.8
5	(0, 2)	15.6	16.3	19.7	3.1	3.0	4.4
6	(-1, -2)	14.0	11.5	14.3	2.8	2.6	3.4
7	(3, 0)	23.5	21.5	25.4	2.9	3.5	2.9
8	(0, 3)	20.6	17.8	24.1	2.9	2.5	4.3
9	(-3, 0)	24.4	18.7	25.2	2.7	4.0	3.4
10	(0, -3)	10.1	10.0	13.6	1.3	1.6	1.8

verified in mild hyperthermia, where the heating in the most of the heated healthy tissue does never exceed the 41-42°C, which is the temperature above which the blood perfusion change significantly with the temperature [27]) above result entails that for a temperature increase in the tumor of 5°C, a temperature raise not larger than 2 °C is expected in the healthy tissue (i.e., 39 °C), which is well tolerated. This conclusion is reinforced by the fact that the secondary maxima of $p_e(\mathbf{r})$ occur at the breast periphery-see Fig. 3-, where the heat exchange with the refrigerant BM is expected being more effective.

For tumor positions 1 and 10, a smaller *SL* is obtained, indicating the presence of a larger secondary peak of $p_e(\mathbf{r})$, as confirmed by the maps in Fig. 3. This happens essential because the focusing is unconstrained, therefore, it does not assure the absence of significant secondary peaks of $p_e(\mathbf{r})$, especially for tumors near or embedded in a high loss region, as for the case under consideration. However, as already pointed out, this is a drawback common to all the unconstrained approaches, confirmed by the fact that we found this behavior also for the TR approach. From Table I one can also notice that, unlike *D*, the highest *SL* is not always obtained for the TR approach. This is not surprising because, the TR approach maximizes *D*, but not *SL*.

To complete the study, we have analyzed the robustness of both strategies A and B against the measurement noise. This has been carried out by adding to $\underline{\underline{S}}$ a NxN random matrix, with complex Gaussian entries, having zero mean. The performance have been evaluated by estimating *D* and *SL* as a function of SNR, defined as the squared ratio of the L_2 norms of $\underline{\underline{S}}$ and of the random matrix simulating the noise. The results are reported in Fig. 5 for the tumor position (and size) in Fig. 2. Panel (a) shows the results for *D*, while panel (b) the results for *SL*. As it can be seen, both *D* and *SL* exhibit a drop (a reduction of about one half with respect to the value in absence of noise) occurring at $\mathrm{SNR_A} \approx 15$ dB, for strategy, A and $\mathrm{SNR_B} \approx 20$ dB for strategy B. This means that, at least for the case at hand, to be effective, strategy A requires a noise level at least 15 dB below the level of $\underline{\underline{S}}$, while strategy B requires a noise level at least 20 dB below. In our case, the level of the differential scattering matrix $\underline{\underline{S}}$ turns out to be about 56 dB below that of the scattering matrix itself. Hence, we need a noise level not larger than -56-$\mathrm{SNR_{A[B]}}$,

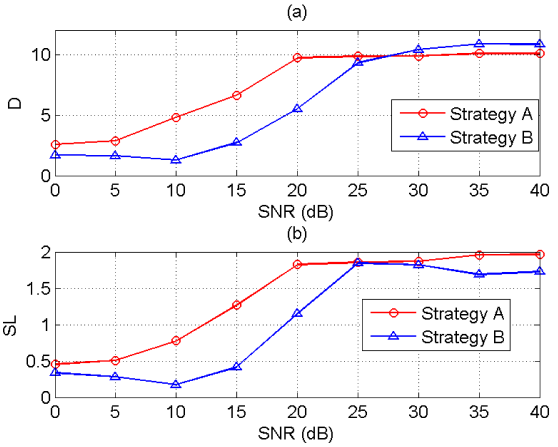

FIGURE 5. Behavior of *D* (a) and *SL* (b) versus SNR.

namely -71 dB for strategy A and -76 dB for strategy B, with respect to the scattering matrix. Of course, the above values of noise level can be increased of an amount equal to $(m/m_0)_{\mathrm{dB}}$ if one exploits a larger dosage, m, of MNP, m_0 being the amount assumed in this study (see Sect. IV-B).

The following final remarks are in order.

Strategy B requires a SNR approximately equal to the ratio between the singular value of $\underline{\underline{S}}$ corresponding to the electric dipole (i.e. the third) and the highest one (i.e. the first). This is an expected result, as the level of the electric dipole moment is lower than the level of $\underline{\underline{S}}$ of an amount approximately given by such ratio.

As foreseen, strategy A is more robust against the measurement noise than strategy B, even if it is not so much. This implies that the use of strategy A can be favorable, as compared with strategy B, for very small tumors. However, this advantage vanishes for larger tumor, as shown in Fig. 4(c) where for a tumor of 16 mm in size the ratio of the third and the first value, hence the level of the electric dipole moment of $\underline{\underline{S}}$, increase from one tenth to about one third (about 10 dB).

D. 3D RESULTS

Fig. 6 shows the (normalized) power distribution dissipated in the breast in three different cuts crossing the tumor center. In particular, panels (a)-(c) are relative to strategy A;

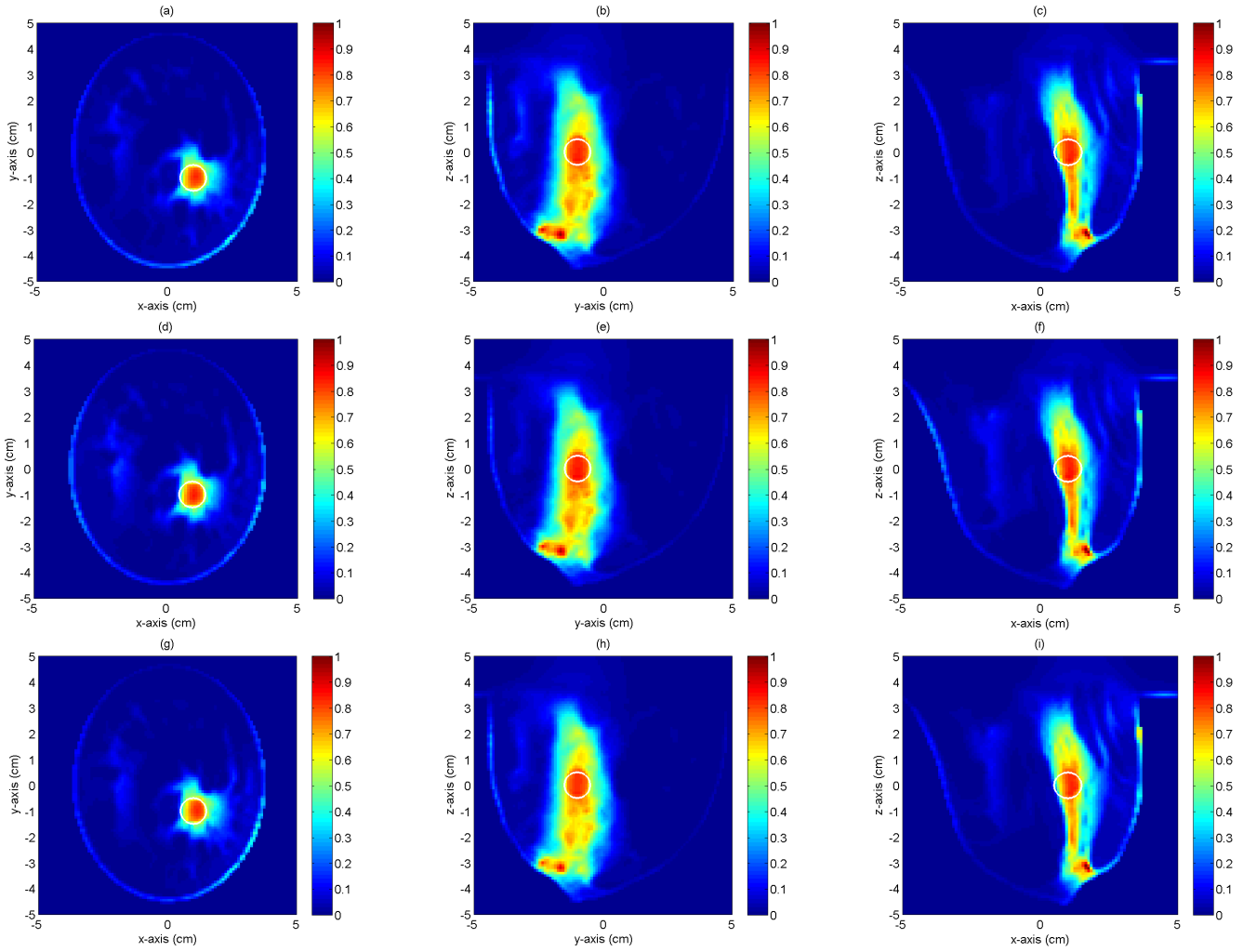

FIGURE 6. Normalized electric power distribution dissipated in the 3D breast model. Strategy A: (a) x=0 cm cut plane; (b) y=0 cm cut plane; (c) z=−2 cm cut plane. Strategy B: (d) x=0 cm cut plane; (e) y=0 cut plane cm; (f) z=−2 cm cut plane. TR: (g) x=0 cm cut plane; (h) y=0 cut plane cm; (i) z=−2 cm cut plane. White circles delimit the tumor.

panels (d)-(f) are relative to strategy B. For comparison, in panels (g)-(i), we show the results obtained by applying the TR approach.

From these results one can immediately notice that in all cases, a good focusing is obtained in the z=0 cut (see panels (a), (d) and (g)), i.e. in the plane where the antenna array lies, while the focusing worsens in the other (i.e. orthogonal) planes. This degradation is obviously due to the fact that an array consisting of only one ring of antennas has been adopted, and can be counteracted by employing more antennas rings, lying on different z planes.

The most interesting outcome is that even in this realistic 3D case, our results compare very well with those obtained through the TR approach, as corroborated by the comparison of the antenna excitations, shown in Fig. 7.

This further confirms the fact that the worse focusing observed in some directions is not due to a failure of the proposed strategies, but rather is intrinsic to the considered set- up (i.e. number, type, position and orientation of the antennas, working frequency, BM and so on).

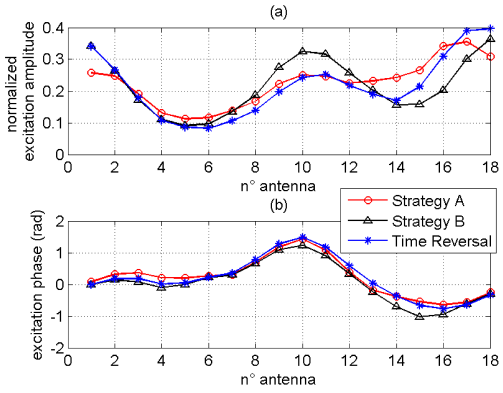

FIGURE 7. Normalized amplitudes (a) and phases (b) of the antenna excitations in the case of 3D breast model.

Another interesting outcome is that the antenna coupling (at least for the considered antennas) does not affect the effectiveness of the proposed strategies. This was to be expected, because the case of an actual array differs from

the case of ideal sources for the fact that in the former case the BM is no longer homogeneous, but characterized by the presence of scatterers, namely the antennas and the array structure. However, this presence is reflected in the measured scattering matrix, and so it automatically taken into account in our blind approach, and has no effect on the capability of the devised strategies to estimate the right antenna excitations.

Of course, what could change are the focusing performance, so that a future study on the influence of the kind of antennas and of the array layout is certainly worthy.

V. CONCLUSIONS

A new approach to blind MH, exploiting MNP as contrast agents, has been investigated and numerically validated. In this approach, the antenna excitations are determined by measuring the DSM resulting from the contrast variation of the MNP in the tumor induced by an applied PMF.

The main advantage of this solution is that the change of the magnetic contrast of the MNP is obtained, in a fast, remote and reversible manner. This makes the focusing of the EF on the tumor much more robust with respect to unwanted variations of the electric scenario due to, for instance, to the patient's life activities. Moreover, it allows a continuous tuning of the antenna excitations, hence a reconfigurable focusing of the EF, to counteract possible loss of focusing due to changes of the electric scenario of the ROI during the treatment, in particular those due to the temperature variations.

The magnetic character of the induced contrast has required the development of *ad hoc* strategies for the synthesis of the excitations, which, together with the use of the MNP, represent the novelty of the proposed approach.

The results of an exhaustive 2D numerical analysis, carried out by employing a slice of realistic breast model, have shown the effectiveness of the approach for several tumor positions in the breast, as well as its robustness against measurement noise.

The effectiveness of the approach has been confirmed by a 3D analysis carried out by exploiting an accurate breast model and realistic antennas.

In conclusion, it is worth noting that, while the proposed approach enables the blind and reconfigurable focusing of the electric power on the tumor, it does not allow one to predict the input power required to heat up the tumor above the therapeutic temperature. Therefore, a continuous monitoring of the temperature during the treatment, to provide feedback for the determination of required input power, is mandatory also in this case, as always happens in hyperthermia. However, in this case only one thermometric probe, inserted in the tumor is required.

Future work will concern the assessment of the performance of the approach, in full 3D realistic case, for different set up and conditions (i.e. by varying the breast model, the tumor size, the working frequency, the BM, type of antennas), including the thermal analysis. The ultimate goal will be an experimental assessment of the effectiveness of the proposed approach.

APPENDIX

In this appendix we derive the expression of the element $s_{n,m}$ of the matrix $\underline{\underline{S}}$ given in (6). To this end, let us start by putting in (5) $\Psi_{m,n}(\mathbf{r}) = \mathbf{H}^i_m(\mathbf{r}) \cdot \mathbf{H}^i_n(\mathbf{r})$, so that:

$$s_{m,n} = \int_{\Omega t} \chi(\mathbf{r})\, \Psi_{m,n}(\mathbf{r})\, d\mathbf{r} \tag{A.1}$$

By expanding $\Psi_{m,n}(\mathbf{r})$ in Maclaurin's series and truncating the expansion to the second order term in $\mathbf{r}$, one has:

$$s_{m,n} \cong \Psi_{m,n}(\mathbf{0}) \int_{\Omega t} \chi(\mathbf{r})\, d\mathbf{r} + \nabla\Psi_{m,n}(\mathbf{0}) \cdot \int_{\Omega t} \chi(\mathbf{r})\, \mathbf{r} d\mathbf{r} + \frac{1}{2} \int_{\Omega t} \chi(\mathbf{r})\, \mathbf{r} \cdot \underline{\underline{\partial}}^2 \Psi_{m,n}(\mathbf{0}) \cdot \mathbf{r} d\mathbf{r} \tag{A.2}$$

$\nabla\Psi_{m,n}$ and $\underline{\underline{\partial}}^2\Psi_{m,n}$ being the gradient and the Hessian matrix of $\Psi_{m,n}$, respectively.

Now, by recalling that the origin of the fixed reference frame is assumed coincident with the barycenter of $\chi(\mathbf{r})$, in (A.1) the linear term in $\mathbf{r}$ disappears, so that, after some mathematical steps, $s_{m,n}$ becomes:

$$s_{m,n} \cong \int_{\Omega t} \chi(\mathbf{r}) d\mathbf{r} \left(\Psi_{m,n}(\mathbf{0}) + \frac{1}{2} \sum\nolimits_{q=1}^{3} \mathbf{i_q} \cdot \underline{\underline{X}} \cdot \underline{\underline{\partial}}^2 \Psi_{m,n}(\mathbf{0}) \cdot \mathbf{i_q} \right) \tag{A.3}$$

where $\underline{\underline{X}}$ is the 3×3 matrix given by:

$$\underline{\underline{X}} = \frac{\int_{\Omega t} \chi(\mathbf{r})\, \mathbf{r}\mathbf{r} d\mathbf{r}}{\int_{\Omega t} \chi(\mathbf{r})\, d\mathbf{r}} \tag{A.4}$$

In the case of a spherically symmetric distribution of MNP (i.e. $\chi(r) = \chi(r)$), the integral giving $\underline{\underline{X}}$ reduces to:

$$\underline{\underline{X}} = \frac{\int_{\Omega t} \chi(\mathbf{r}) \mathbf{r}\mathbf{r} d\mathbf{r}}{\int_{\Omega t} \chi(\mathbf{r}) d\mathbf{r}} = \frac{-2\pi \int_o^{\pi} \cos^2\vartheta d\cos\vartheta \int_0^{R_t} \chi(r) r^4 dr}{2\pi \int_o^{\pi} \sin\vartheta d\vartheta \int_0^{R_t} \chi(r) r^2 dr} \underline{\underline{I}} = \frac{1}{3} \frac{\int_0^{R_t} \chi(r) r^4 dr}{\int_0^{R_t} \chi(r) r^2 dr} d\underline{\underline{I}} = \frac{1}{5} R^2 \underline{\underline{I}} \tag{A.5}$$

$\underline{\underline{I}}$ being the 3×3 identity matrix and R an "effective" radius of the MNP distribution, whose maximum value (attained in the case of a uniform distribution) is equal to the radius, R_t, of Ω_t. By replacing (A.5) in (A.3) and recalling that $\Psi_{m,n}(\mathbf{r}) = \mathbf{H}^i_m(\mathbf{r}) \cdot \mathbf{H}^i_n(\mathbf{r})$, one obtains:

$$s_{m,n} \cong \int_{\Omega t} \chi(\mathbf{r}) d\mathbf{r} \left(\mathbf{H}^i_m(\mathbf{0}) \cdot \mathbf{H}^i_n(\mathbf{0}) + \frac{R^2}{10} \nabla^2 \left(\mathbf{H}^i_m \cdot \mathbf{H}^i_n \right)(\mathbf{0}) \right) \tag{A.6}$$

from which, by developing the Laplacian of the dot product of the MF, one has:

$$s_{m,n} \cong \int_{\Omega t} \chi(\mathbf{r})\, d\mathbf{r} (\mathbf{H}^i_m(\mathbf{0}) \cdot \mathbf{H}^i_n(\mathbf{0}) + \frac{R^2}{10} \mathbf{H}^i_m(\mathbf{0}) \cdot \nabla^2 \mathbf{H}^i_n(\mathbf{0}) + \frac{R^2}{10} \nabla^2 \mathbf{H}^i_m(\mathbf{0}) \cdot \mathbf{H}^i_n(\mathbf{0}) + \frac{R^2}{5} \sum\nolimits_{q=1}^{3} (\mathbf{i_q} \cdot \nabla \mathbf{H}^i_m(\mathbf{0})) \cdot (\mathbf{i_q} \cdot \nabla \mathbf{H}^i_n(\mathbf{0})) \tag{A.7}$$

The second and the third terms in (A.7) can be further recast by exploiting the Maxwell's equations. Concerning the second term in (A.7), it results:

$$\nabla^2 \mathbf{H}^i_{\mathrm{m[n]}}(\mathbf{0}) = -k_t^2 \mathbf{H}^i_{\mathrm{m[n]}}(\mathbf{0}) - i\omega \nabla\varepsilon(\mathbf{0}) \times \mathbf{E}^i_{\mathrm{m[n]}}(\mathbf{0}) \quad \text{(A.8)}$$

k_t being the propagation constant of the medium at $\mathbf{r}=\mathbf{0}$. On the right hand of (A.8), the term related to the EF can be neglected if its amplitude is much smaller than the amplitude of the term related to the MF. This happens when $|\nabla\varepsilon(\mathbf{0})| / |k_t \varepsilon(\mathbf{0})| \ll 1$, which is quite verified for the cases and the frequencies of interest in FMH. Therefore, $\mathrm{s_{m,n}}$ assumes the form:

$$\begin{aligned} \mathrm{s_{m,n}} \cong & \left(1 - \frac{1}{5}(k_\mathrm{t}R)^2\right) \int_{\Omega\mathrm{t}} \chi(\mathbf{r})\, d\mathbf{r} \mathbf{H}^i_\mathrm{m}(\mathbf{0}) \cdot \mathbf{H}^i_\mathrm{n}(\mathbf{0}) \\ & + \frac{R^2}{5} \int_{\Omega\mathrm{t}} \chi(\mathbf{r})\, d\mathbf{r} \sum\nolimits_{\mathrm{q}=1}^{3} \left(\mathbf{i_q} \cdot \nabla \mathbf{H}^i_\mathrm{m}(\mathbf{0})\right) \\ & \cdot \left(\mathbf{i_q} \cdot \nabla \mathbf{H}^i_\mathrm{n}(\mathbf{0})\right) \end{aligned} \quad \text{(A.9)}$$

Concerning the third term in (A.7), by splitting $\nabla \mathbf{H}^i_{\mathrm{n[m]}}(\mathbf{0})$ into its symmetric, $\nabla_s \mathbf{H}^i_{\mathrm{n[m]}}(\mathbf{0})$, and anti-symmetric, $\nabla_a \mathbf{H}^i_{\mathrm{n[m]}}(\mathbf{0})$, and exploiting the results [28]:

$$\begin{aligned} & = \sum\nolimits_{\mathrm{q}=1}^{3} \left(\mathbf{i_q} \cdot \nabla_a \mathbf{H}^i_\mathrm{m}(\mathbf{0})\right) \cdot \left(\mathbf{i_q} \cdot \nabla_s \mathbf{H}^i_\mathrm{n}(\mathbf{0})\right) \\ & = \sum\nolimits_{\mathrm{q}=1}^{3} \left(\mathbf{i_q} \cdot \nabla_a \mathbf{H}^i_\mathrm{n}(\mathbf{0})\right) \cdot \left(\mathbf{i_q} \cdot \nabla_s \mathbf{H}^i_\mathrm{m}(\mathbf{0})\right) = 0 \end{aligned} \quad \text{(A.10)}$$

$$\begin{aligned} \mathbf{i_q} \cdot \nabla_a \mathbf{H}^i_{\mathrm{m[n]}}(\mathbf{0}) &= \mathbf{i_q} \times \nabla \times \mathbf{H}^i_{\mathrm{m[n]}}(\mathbf{0}) \\ &= \frac{\mathbf{1}}{2} i\omega\varepsilon(\mathbf{0})\, \mathbf{i_q} \times \mathbf{E}^i_{\mathrm{m[n]}}(\mathbf{0}) \end{aligned} \quad \text{(A.11)}$$

we get:

$$\begin{aligned} & \left(\nabla \mathbf{H}^i_\mathrm{m}(\mathbf{0}) \cdot \mathbf{i_q}\right) \cdot \left(\nabla \mathbf{H}^i_\mathrm{n}(\mathbf{0}) \cdot \mathbf{i_q}\right) \\ & = -\frac{k_\mathrm{t}^2}{4\zeta_\mathrm{t}^2} \mathbf{i_q} \times \mathbf{E}^i_\mathrm{m}(\mathbf{0}) \cdot \mathbf{i_q} \times \mathbf{E}^i_\mathrm{n}(\mathbf{0}) \\ & \quad + \frac{\mathbf{1}}{\mathbf{4}} \mathbf{i_q} \cdot \nabla_s \mathbf{H}^i_\mathrm{m}(\mathbf{0}) \cdot \nabla_s \mathbf{H}^i_\mathrm{n}(\mathbf{0}) \cdot \mathbf{i_q} \end{aligned} \quad \text{(A.12)}$$

being ζ_t the characteristic impedance of the medium at $\mathbf{r}=0$. By circularly permuting the dot-cross product in (A.12) and replacing in (A.9), after some mathematical steps, $\mathrm{s_{m,n}}$ becomes:

$$\begin{aligned} \mathrm{s_{m,n}} \cong & \int_{\Omega\mathrm{t}} \chi(\mathbf{r})\, d\mathbf{r} \left((1 - \frac{1}{5}(k_\mathrm{t}R)^2) \mathbf{H}^i_\mathrm{m}(\mathbf{0}) \cdot \mathbf{H}^i_\mathrm{n}(\mathbf{0}) \right. \\ & - \frac{(k_\mathrm{t}R)^2}{10\zeta_\mathrm{t}^2} \mathbf{E}^i_\mathrm{m}(\mathbf{0})^\mathrm{T} \cdot \mathbf{E}^i_\mathrm{n}(\mathbf{0}) + \frac{(k_\mathrm{t}R)^2}{20k_\mathrm{t}^2} \sum\nolimits_{\mathrm{q}=1}^{3} \mathbf{i_q} \\ & \left. \cdot \nabla_s \mathbf{H}^i_\mathrm{m}(\mathbf{0}) \cdot \nabla_s \mathbf{H}^i_\mathrm{n}(\mathbf{0}) \cdot \mathbf{i_q} \right) \end{aligned} \quad \text{(A.13)}$$

namely, the expression of $\mathrm{s_{m,n}}$ given in (6).

ACKNOWLEDGMENTS

The authors would like to thank the Computer Simulation Technology AG, Darmstadt, Germany, for having provided us with a trial version of the CST MWS 2016, employed to perform the 3D simulations reported in this work

REFERENCES

[1] J. Stang, M. Haynes, P. Carson, and M. Moghaddam, "A preclinical system prototype for focused microwave thermal therapy of the breast," *IEEE Trans. Biomed. Eng.*, vol. 59, no. 9, pp. 2431–2438, Sep. 2012.
[2] P. Togni *et al.*, "Electromagnetic redesign of the HYPERcollar applicator: Toward improved deep local head-and-neck hyperthermia," *Phys. Med. Biol.*, vol. 58, pp. 5997–6009, Aug. 2013.
[3] J. de Rosny, G. Lerosey, and M. Fink, "Theory of electromagnetic time-reversal mirrors," *IEEE Trans. Antennas Propag.*, vol. 58, no. 10, pp. 3139–3149, Oct. 2010.
[4] H. D. Trefná, J. Vrba, and M. Persson, "Time-reversal focusing in microwave hyperthermia for deep-seated tumors," *Phys. Med. Biol.*, vol. 55, pp. 2167–2185, Apr. 2010.
[5] A. Boag and Y. Leviatan, "Optimal excitation of multiapplicator systems for deep regional hyperthermia," *IEEE Trans. Biomed. Eng.*, vol. 37, no. 10, pp. 987–995, Oct. 1990.
[6] F. Bardati, A. Borrani, A. Gerardino, and G. A. Lovisolo, "SAR optimization in a phased array radiofrequency hyperthermia system," *IEEE Trans. Biomed. Eng.*, vol. 42, no. 12, pp. 1201–1207, Dec. 1995.
[7] K. S. Nikita, N. G. Maratos, and N. K. Uzunoglu, "Optimization of the deposited power distribution inside a layered lossy medium irradiated by a coupled system of concentrically placed waveguide applicators," *IEEE Trans. Biomed. Eng.*, vol. 45, no. 7, pp. 909–920, Jul. 1998.
[8] D. A. M. Iero, T. Isernia, A. F. Morabito, I. Catapano, and L. Crocco, "Optimal constrained field focusing for hyperthermia cancer therapy: A feasibility assessment on realistic phantoms," *Prog. Electromagn. Res.*, vol. 102, pp. 125–141, Mar. 2010.
[9] M. J. Burfeindt, E. Zastrow, S. C. Hagness, B. D. Van Veen, and J. E. Medow, "Microwave beamforming for non-invasive patient-specific hyperthermia treatment of pediatric brain cancer," *Phys. Med. Biol.*, vol. 56, pp. 2743–2754, May 2011.
[10] P. T. Nguyen, A. Abbosh, and S. Crozier, "Microwave hyperthermia for breast cancer treatment using electromagnetic and thermal focusing tested on realistic breast models and antenna arrays," *IEEE Trans. Antennas Propag.*, vol. 63, no. 10, pp. 4426–4434, Oct. 2015.
[11] G. Bellizzi and O. M. Bucci, "Blind focusing of electromagnetic fields in hyperthermia exploiting target contrast variations," *IEEE Trans. Biomed. Eng.*, vol. 62, no. 1, pp. 208–217, Jan. 2015.
[12] G. Bellizzi, O. M. Bucci, and I. Catapano, "Microwave cancer imaging exploiting magnetic nanoparticles as contrast agent," *IEEE Trans. Biomed. Eng.*, vol. 58, no. 9, pp. 2528–2536, Sep. 2011.
[13] G. Bellizzi and O. M. Bucci, "Blind focusing of the electric field in microwave hyperthermia exploiting magnetic nanoparticles," in *Proc. 11th EuCAP*, Paris, France, Mar. 2017, pp. 2751–2753.
[14] *Magnetic Hyperthermia*. MagForce AG, Berlin, Germany. [Online]. Available: http://www.magforce.de/en/unternehmen/ueber-uns.html
[15] O. M. Bucci, G. Bellizzi, and G. G. Bellizzi, "Microwave broadband characterization of a diluted water-based ferrofluid in presence of a polarizing magnetic field," *IEEE Trans. Magn.*, vol. 53, no. 3, Mar. 2017, Art. no. 5300108.
[16] G. Bellizzi and O. M. Bucci, "A novel measurement technique for the broadband characterization of diluted water ferrofluids for biomedical applications," *IEEE Trans. Magn.*, vol. 49, no. 6, pp. 2903–2912, Jun. 2013.
[17] G. H. Golub and C. F. Van Loan, *Matrix Computations*. Baltimore, MD, USA: The Johns Hopkins Univ. Press, 1996.
[18] A. A. Golneshan and M. Lahonian, "Diffusion of magnetic nanoparticles in a multi-site injection process within a biological tissue during magnetic fluid hyperthermia using lattice Boltzmann method," *Mech. Res. Commun.*, vol. 38, pp. 425–430, Sep. 2011.
[19] O. M. Bucci, L. Crocco, R. Scapaticci, and G. Bellizzi, "On the design of phased arrays for medical applications," *Proc. IEEE*, vol. 104, no. 3, pp. 633–648, Mar. 2016.
[20] O. M. Bucci, C. Gennarelli, and C. Savarese, "Representation of electromagnetic fields over arbitrary surfaces by a finite and nonredundant number of samples," *IEEE Trans. Antennas Propag.*, vol. 46, no. 3, pp. 351–359, Mar. 1998.
[21] K. Maier-Hauff *et al.*, "Efficacy and safety of intratumoral thermotherapy using magnetic iron-oxide nanoparticles combined with external beam radiotherapy on patients with recurrent glioblastoma multiforme," *J. Neuro-Oncol.*, vol. 103, no. 2, pp. 317–324, 2011.
[22] M. Johannsen, B. Thiesen, P. Wust, and A. Jordan, "Magnetic nanoparticle hyperthermia for prostate cancer," *Int. J. Hyperthermia*, vol. 26, no. 8, pp. 790–795, Aug. 2010.

[23] S. Ley, M. Helbig, and J. Sachs, "Preliminary investigations of magnetic modulated nanoparticles for microwave breast cancer detection," *Current Directions Biomed. Eng.*, vol. 1, pp. 302–305, 2015.
[24] O. M. Bucci, G. Bellizzi, S. Costanzo, L. Crocco, G. Di Massa, and R. Scapaticci, "Towards the assessment of detection limits in magnetic nanoparticle enhanced microwave imaging of breast cancer," in *Proc. 11th EuCAP*, Paris, France, Mar. 2017, pp. 3489–3492.
[25] E. Zastrow, S. K. Davis, M. Lazebnik, F. Kelcz, B. D. Van Veem, and S. C. Hagness. *Database of 3D Grid-Based Numerical Breast Phantom for Use in Computational Electromagnetic Simulations*. Accessed on 2007. [Online]. Available: https://uwcem.ece.wisc.edu/index.html
[26] M. Lazebnik *et al.*, "A large-scale study of the ultrawideband microwave dielectric properties of normal, benign and malignant breast tissues obtained from cancer surgeries," *Phys. Med. Biol.*, vol. 52, pp. 6093–6115, Oct. 2007.
[27] G. Bellizzi, O. M. Bucci, and G. Chirico, "Numerical assessment of a criterion for the optimal choice of the operative conditions in magnetic nanoparticle hyperthermia on a realistic model of the human head," *Int. J. Hyperthermia*, vol. 32, pp. 688–703, Sep. 2016.
[28] C. H. Papas, *Theory of Electromagnetic Wave Propagation*. New York, NY, USA: Dover, 1988.

GENNARO BELLIZZI received the Laurea (*summa cum laude*) degree in telecommunication engineering and the Ph.D. degree in electronic and telecommunication engineering from the University of Naples Federico II, Naples, Italy, in 2004 and 2008, respectively. Since 2008, he has been with the Dipartimento di Ingegneria Elettronica e delle Telecomunicazioni, University of Naples Federico II. His research interests include the analysis and modeling of the interactions mechanisms between electromagnetic fields and nanomachines, the electromagnetic characterization of magnetic nanoparticles and magnetic fluids, magnetic fluid and microwave hyperthermia microwave imaging, and inverse scattering techniques. He received the Sannino Award for Young Scientists at the XVIII Riunione Nazionale di Elettromagnetismo in 2010.

OVIDIO MARIO BUCCI (LF'16) was born in Civitaquana, Italy, in 1943.

He received the (*summa cum laude*) degree in electronic engineering from the Universiy of Naples in 1966, and the Libera Docenza degree in theory and technique of electromagnetic fields (becoming a tenured University Professor) in 1971. He was an Assistant Professor with the Istituto Universitario Navale of Naples from 1967 to 1975, and then a Full Professor of electromagnetic fields with the University of Naples Federico II from 1976 to 2014. He was the Director of the Department of Electronic Engineering from 1984 to 1986 and 1989 to 1990, the Vice-Rector of the University of Naples Federico II from 1994 to 2000, and the Director of the CNR Institute of Electromagnetic Environmental Sensing from 2001 to 2010. He is currently a Professor Emeritus with the University of Naples Federico II. He is member of the Board of the European School of Antennas. He was also the President of the National Research Group of Electromagnetism, the MTT-AP Chapter of the Center-South Italy Section of the IEEE, and the Director of the Interuniversity Research Center on Microwaves and Antennas.

He has authored or co-authored over 400 scientific papers, mainly published in international scientific journals or conference proceedings. His scientific interests include scattering from loaded surfaces, reflector and array antennas, efficient representations of electromagnetic fields, near-field far-field measurement techniques, inverse problems and noninvasive diagnostics, and the biological applications of nanoparticles and electromagnetic fields.

He was a recipient of the International Award GUIDO DORSO for Scientific Research in 1996, and the Presidential Gold Medal for Science and Culture in 1998. He is a member of the Academia Pontaniana.